

Established conversions for hybrid entangled states assisted by error-predicted parity-discriminated devices

Fang-Fang Du(杜芳芳), Zhi-Guo Fan(范志国), Xue-Mei Ren(任雪梅), Ming Ma(马明), and Wen-Yao Liu(刘文耀)
Citation: Chin. Phys. B, 2025, 34 (**1**): 010303. DOI: 10.1088/1674-1056/ad8fa0
Journal homepage: http://cpb.iphy.ac.cn; http://iopscience.iop.org/cpb

What follows is a list of articles you may be interested in

Exact quantum dynamics for two-level systems with time-dependent driving

Zhi-Cheng He(贺郅程), Yi-Xuan Wu(吴奕璇), and Zheng-Yuan Xue(薛正远)
Chin. Phys. B, 2024, 33 (**12**): 120310. DOI: 10.1088/1674-1056/ad8a4c

Generation of macroscopic entanglement in ensemble systems based on silicon vacancy centers

Jian-Zhuang Wu(武建壮), Ying Xi(奚滢), Bo-Ya Li(李博雅), Lian-E Lu(芦连娥), and Yong-Hong Ma(马永红)
Chin. Phys. B, 2024, 33 (**9**): 090308. DOI: 10.1088/1674-1056/ad5d93

Simulations of superconducting quantum gates by digital flux tuner for qubits

Xiao Geng(耿霄), Kaiyong He(何楷泳), Jianshe Liu(刘建设), and Wei Chen(陈炜)
Chin. Phys. B, 2024, 33 (**7**): 070305. DOI: 10.1088/1674-1056/ad47ab

Quantum correlations and entanglement in coupled optomechanical resonators with photon hopping via Gaussian interferometric power analysis

Y. Lahlou, B. Maroufi, and M. Daoud
Chin. Phys. B, 2024, 33 (**5**): 050303. DOI: 10.1088/1674-1056/ad2a6e

Enhanced measurement precision with continuous interrogation during dynamical decoupling

Jun Zhang(张军), Peng Du(杜鹏), Lei Jing(敬雷), Peng Xu(徐鹏), Li You(尤力), and Wenxian Zhang(张文献)
Chin. Phys. B, 2024, 33 (**3**): 030301. DOI: 10.1088/1674-1056/ad1985

SPECIAL TOPIC — Quantum communication and quantum network

Established conversions for hybrid entangled states assisted by error-predicted parity-discriminated devices

Fang-Fang Du(杜芳芳)[†], Zhi-Guo Fan(范志国), Xue-Mei Ren(任雪梅), Ming Ma(马明), and Wen-Yao Liu(刘文耀)[‡]

Science and Technology on Electronic Test and Measurement Laboratory, North University of China, Taiyuan 030051, *China*

(Received 1 September 2024; revised manuscript received 27 October 2024; accepted manuscript online 7 November 2024)

Hybrid entangled states are crucial in quantum physics, offering significant benefits for hybrid quantum communication and quantum computation, and then the conversion of hybrid entangled states is equally critical. This paper presents two novel schemes, that is, one converts the two-qubit hybrid Knill–Laflamme–Milburn (KLM) entangled state into Bell states and the other one transforms the three-qubit hybrid KLM state into Greenberger–Horne–Zeilinger (GHZ) states assisted by error-predicted and parity-discriminated devices. Importantly, the integration of single photon detectors into the parity-discriminated device enhances predictive capabilities, mitigates potential failures, and facilitates seamless interaction between the nitrogen-vacancy center and photons, so the two protocols operate in an error-predicted way, improving the experimental feasibility. Additionally, our schemes demonstrate robust fidelities (close to 1) and efficiencies, indicating their feasibility with existing technology.

Keywords: quantum information processing, quantum entanglement, quantum communication, entanglement conversion

PACS: 03.67.–a, 03.67.Hk, 03.67.Dd, 03.65.Ud

DOI: 10.1088/1674-1056/ad8fa0 **CSTR:** 32038.14.CPB.ad8fa0

1. Introduction

Quantum entanglement, as a cornerstone of quantum theory, plays an essential role in a variety of advanced quantum information processing (QIP).[1–6] This phenomenon underpins numerous functionalities in quantum networks, including distributed quantum computation,[7–11] quantum key distribution,[12–15] quantum teleportation,[16–20] and quantum secure direct communication.[21–33] The foundational nature of quantum entanglement underscores its importance in both theoretical and practical aspects of these technologies. The Bell state, Greenberger–Horne–Zeilinger (GHZ) state,[34] W state,[35] and Knill–Laflamme–Milburn (KLM) state[36] are commonly studied forms of quantum entangled states and the direct preparations of these entangled states are of great significance for QIP. In multi-qubit systems utilizing KLM and W states, the loss of a single qubit does not necessarily compromise the entanglement of the remaining qubits, which may retain entanglement with a certain probability.[37,38] This characteristic helps to reduce the bit error rate and provides unique benefits for linear optical quantum information processing. In contrast, the GHZ state displays properties that underscore the differences between quantum mechanics and classical theories of local hidden variables, deteriorating completely upon the loss of any single qubit.[39–45] The direct preparation and conversion of entangled states are paramount in the realm of quantum engineering.

The KLM and GHZ entangled states represent two distinct categories of multi-qubit entanglement, which are not interconvertible via local operations and classical communication.[46–48] This has sparked considerable interest in their direct conversion. Furthermore, since KLM and GHZ states can perform different QIP tasks, this raises the question of how to convert one entangled state into the other, which is the motivation behind the development of our conversion protocol. Prior studies have demonstrated the feasibility of transforming KLM states into W states and W states into GHZ states.[49–51] However, the conversion efficiency through the intermediary W state remains notably low. In recent years, protocols for directly converting KLM states into GHZ states have undergone significant development.[52–54] Nevertheless, existing methods for direct conversion from KLM to GHZ states are confined to either purely photonic or solid-state qubits, without addressing general hybrid states. The hybrid system we designed, consisting of photons and solid-state quantum qubits, offers a pioneering platform for QIP. It enables an innovative and efficient conversion scheme designed specifically for hybrid entangled states, and can be regarded as a valuable addition to entangled state preparation.

Solid-state spin systems have emerged as a promising experimental platform for quantum qubit encoding.[55–58] Electron spin in the negatively charged nitrogen-vacancy (NV^-) center is particularly noteworthy within this context.[59–62]

[†]Corresponding author. E-mail: Duff@nuc.edu.cn

[‡]Corresponding author. E-mail: liuwenyao@nuc.edu.cn

© 2025 Chinese Physical Society and IOP Publishing Ltd. All rights, including for text and data mining, AI training, and similar technologies, are reserved.

The NV^- center facilitates easier optical initialization, enables single-qubit operations, and provides high-fidelity readout at room temperature.[63,64] Moreover, it manages the millisecond coherence times of NV^- center electron spins through spin echo techniques. The NV^- centers have been instrumental in developing various applications, including distributed quantum computing and hybrid quantum gates that influence both electron spins and nearby nuclear spins.[65,66] They have also been used to create geometric single qubit gates,[67–69] CNOT gates,[70–72] and universal multi-qubit gates encoding on both electron and photon qubits of NV^- centers.[73–78] Recent advances have proposed entanglement and hyper-entanglement purification techniques using NV^- center emissions.[79] Building upon this groundwork, we intend to utilize hybrid photon-NV^- center for converting KLM state to GHZ states.

Inspired by prior researches, we introduce two innovative protocols in this paper, that is, the first one converts two-qubit hybrid KLM state into hybrid Bell states, while the second one transforms three-qubit hybrid KLM state into hybrid GHZ states via the error-predicted parity-discriminated devices (EPPDD). The implementation of EPPDD in these conversion processes enhances accuracy by monitoring and rectifying errors from photon–NV^- interactions. Our analytical evaluations suggest that these conversions achieve nearly perfect fidelities and high efficiencies, substantially enriching our understanding of hybrid entanglement properties. What is more, the robust fidelities and efficiencies suggest potential feasibility with existing technology.

2. NV^- center configuration

In the advancement of quantum information, it is imperative to establish the relationship between a single photon and individual spins.[80] As illustrated in Fig. 1, the charged NV^- center system in a single-sided optical cavity establishes this connection. The NV^- center system is comprised of a vacancy, a substituted nitrogen atom, and six electrons from both nitrogen and carbon atoms. The intricate interplay between electron–nuclear coupling and optical transitions renders the energy level structure of this system exceptionally complex.

As shown in Fig. 1, under the influence of spin–spin interactions, there exists a zero-field splitting of 2.88 GHz in the ground states between $|0\rangle$ ($m_s = 0$) and $|\pm 1\rangle$ ($m_s = \pm 1$) of the NV^- center. Furthermore, upon applying a specific magnetic field along the symmetry axis, which allows for optical transitions of the spin states, the degeneracy of the spin states $m_s = \pm 1$ is lifted, and the energy levels of the ground states $|0\rangle$ and $|+1\rangle$ (simplified as $|1\rangle$) split, represented by Δ as the energy difference between states $|0\rangle$ and $|1\rangle$ at this time.[81–85] When state $|0\rangle$ absorbs a photon with the resonant frequency ω_0 and transitions to the excited state $|M_3\rangle$, since the cavity mode frequency ω_c is close to resonance, the reflection properties of the cavity are completely altered. In contrast, when state $|1\rangle$ absorbs a photon with the resonant frequency ω_0 and transitions to the excited state $|M_5\rangle$, due to significant detuning between the cavity mode frequency ω_c and its transition frequency, the cavity's reflection properties remain unchanged. Consequently, when photons with input frequency ω are introduced, the reflective behavior of the photons within the cavity depends on the state of the negatively charged NV^- center.

According to the rotating wave approximation, the Hamiltonian of the NV^- center system is expressed as

$$H = \omega_s \hat{\sigma}_+ \hat{\sigma}_- + \omega_c \hat{a}^\dagger \hat{a} + \mathrm{i}g(\hat{\sigma}_+ \hat{a} - \hat{a}^\dagger \hat{\sigma}_-), \tag{1}$$

where ω_s refers to the frequency related to the NV^- center. The operators $\hat{\sigma}_+$ and $\hat{\sigma}_-$ facilitate the elevation and reduction of energy levels in the NV^- center, respectively. The operator $\hat{a}$ (or its adjoint $\hat{a}^\dagger$) acts as the annihilation (creation) operator for the cavity field. Moreover, g measures the interaction strength between the single-sided cavity and the NV^- center.

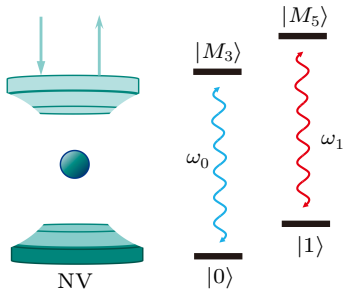


Fig. 1. The coupling system involved an NV^- center and an optical cavity and the structural arrangement of energy levels and optical transitions within the NV^- center.

By solving the dynamics equations of the system and using the standard input–output relations, the reflection coefficient of the NV^-–cavity system can be determined,[86–88] which can be represented as

$$\begin{aligned}
\frac{\mathrm{d}\hat{a}}{\mathrm{d}t} &= -\left[\mathrm{i}(\omega_c - \omega) + \frac{\kappa}{2}\right]\hat{a} - g\hat{\sigma}_- - \sqrt{\kappa}\hat{a}_{\mathrm{in}} + \hat{N}, \\
\frac{\mathrm{d}\hat{\sigma}_-}{\mathrm{d}t} &= -\left[\mathrm{i}(\omega_s - \omega) + \frac{\gamma}{2}\right]\hat{\sigma}_- - g\hat{\sigma}_z\hat{a} + \hat{N}', \\
\hat{a}_{\mathrm{out}} &= \hat{a}_{\mathrm{in}} + \sqrt{\kappa}\hat{a}.
\end{aligned} \tag{2}$$

Noise operators are represented by $\hat{N}$ and $\hat{N}'$, while $\hat{a}_{\mathrm{in}}$ and $\hat{a}_{\mathrm{out}}$ correspond to the input and output field operators, respectively. The decay rates of the cavity field and the excited states of the NV^- center are denoted by κ and γ, respectively. Additionally, $\hat{\sigma}_z = \hat{\sigma}_+\hat{\sigma}_- - \hat{\sigma}_-\hat{\sigma}_+$ serves as the population operator for the NV^- center.

When a photon enters and interacts with the unidirectional cavity–NV^- anion system, under the weak excitation condition ($\langle\hat{\sigma}_z\rangle = -1$), the reflection coefficient $r_s(\omega)$ can be accurately expressed as[89]

$$r_s(\omega) = 1 - \frac{2(1 + \mathrm{i}\Delta_s)}{(1 + \mathrm{i}\Delta_s)(1 + \mathrm{i}\Delta_c) + C}, \tag{3}$$

where subscript $s = 1$ (or $s = 0$) indicates the interaction of a polarized photon with the NV$^-$–cavity system. The parameter $C = 4g^2/(\kappa\gamma)$ quantifies the cooperativity. The terms $\Delta_s = 2(\omega_s - \omega)/\gamma$ and $\Delta_c = 2(\omega_c - \omega)/\kappa$ represent the effective detunings of the dipole and cavity modes, respectively, from the frequency of the input field. Therefore, the interaction between the photon and the unidirectional cavity–NV$^-$ center system can be described as

$$\begin{aligned} |R\rangle|0\rangle &\to r_0(\omega)|R\rangle|0\rangle, \ |R\rangle|1\rangle \to r_1(\omega)|R\rangle|1\rangle, \\ |L\rangle|0\rangle &\to r_1(\omega)|L\rangle|0\rangle, \ |L\rangle|1\rangle \to r_0(\omega)|L\rangle|1\rangle. \end{aligned} \tag{4}$$

3. An error-predicted parity-discriminated device

The transformation from two-qubit hybrid KLM state to hybrid Bell states and that from three-qubit hybrid KLM state into hybrid GHZ states discussed below require the EPPDD illustrated in Fig. 2. Thus, a comprehensive and detailed explanation of the fundamental principle of EPPDD is necessary, which comprises three critical steps.

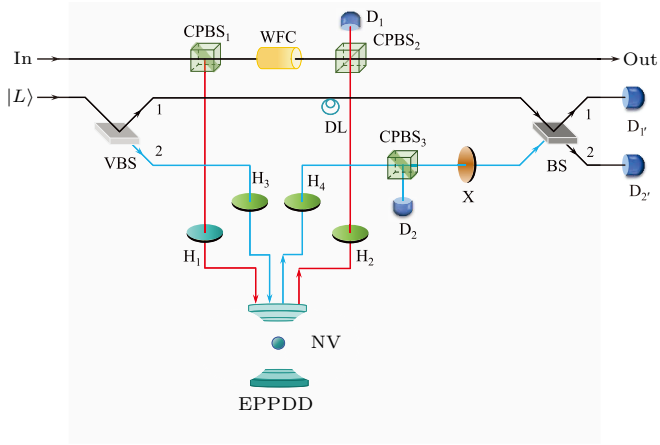


Fig. 2. Schematic diagram of the error-predicted parity-discriminated device (EPPDD). VBS represents a non-equilibrium beam splitter with a transmission coefficient of $(1+M^6)^{-1/2}$ and a reflection coefficient of $M/[(1+M^6)^{-1/2}]$. WFC is a wave-form corrector that performs the transformations $|R\rangle$ ($|L\rangle$) $\to \frac{1}{2}[r_1(\omega) - r_0(\omega)]|R\rangle$ ($|L\rangle$). H$_i$ ($i = 1,2,3,4$) is a half-wave plate that performs Hadamard operation on the polarized photon. CPBS$_i$ ($i = 1,2,3$) represents a circular polarization beam splitter, which transmits the right-polarized photon $|R\rangle$ and reflects the left-polarized photon $|L\rangle$. BS is a 50:50 beam splitter. X is a half-wave plate, which performs bit-flip operation on the photon $\sigma_x^{\rm p} = |R\rangle\langle L| + |L\rangle\langle R|$. Delay line (DL) represents a time-delay device, which can make the photon in two spacial modes output from the device simultaneously. D$_j$ ($j = 1,2,1',2'$) is a single-photon detector.

Assume that the initial electron-spin state of the NV$^-$–cavity system is either $|1\rangle$ or $|0\rangle$, and the state of the input photon is either $|R\rangle$ or $|L\rangle$. In the first step, once the photon is introduced into the EPPDD circuit in path "In", it reaches the first circular polarization beam splitter (CPBS$_1$), which transmits $|R\rangle$-polarized photon and reflects $|L\rangle$-polarized photon. When the photon is in the $|R\rangle$ state, it passes through a wave-form corrector (WFC) that performs the transformation $|R\rangle \to \frac{1}{2}[r_1(\omega) - r_0(\omega)]|R\rangle$. Correspondingly, when the $|L\rangle$-polarized photon input, it goes through a series of processes: H$_1$ $\to$ NV$^-$–cavity system $\to$ H$_2$. H$_i$ ($i = 1,2,3,4$) is a half-wave plate that performs Hadamard operation H$^{\rm p}$ on the photon, i.e., $|R\rangle \xrightarrow{\rm H_1} (|R\rangle - |L\rangle)/\sqrt{2}$, $|L\rangle \xrightarrow{\rm H_1} (|R\rangle + |L\rangle)/\sqrt{2}$, and $|R\rangle \xrightarrow{\rm H_{2,3,4}} (|R\rangle + |L\rangle)/\sqrt{2}$, $|L\rangle \xrightarrow{\rm H_{2,3,4}} (|R\rangle - |L\rangle)/\sqrt{2}$. Notably, the electron spin of the NV$^-$–cavity system needs to execute the Hadamard operation H$^{\rm e}$, i.e., $|1\rangle \to (|1\rangle + |0\rangle)/\sqrt{2}$ and $|0\rangle \to (|1\rangle - |0\rangle)/\sqrt{2}$, both before and after it interacts with the photon. Finally, the photon in different polarized states $|L\rangle$ or $|R\rangle$ merges at CPBS$_2$. Hence, prior to the response of a single-photon detector D$_1$, the hybrid state of the photon and the electron spin evolves into

$$\begin{aligned} &|L\rangle|1\rangle \to M|L\rangle|0\rangle + N|R\rangle|1\rangle, \\ &|L\rangle|0\rangle \to M|L\rangle|1\rangle + N|R\rangle|0\rangle, \\ &|R\rangle|1\rangle \to M|R\rangle|1\rangle, \\ &|R\rangle|0\rangle \to M|R\rangle|0\rangle, \end{aligned} \tag{5}$$

where the parameters M and N represent $\frac{1}{2}[r_1(\omega) - r_0(\omega)]$ and $\frac{1}{2}[r_1(\omega) + r_0(\omega)]$, respectively. As shown in Eq. (5), we can obtain that regardless of the electronic state, the photon state $|L\rangle$ consistently displays two different output modes. In detail, when the state of the output photon is $|R\rangle$, it triggers detector D$_1$, marking a failure event that diminishes efficiency but the electron-spin state of the NV$^-$-cavity system remains unaltered, readying for reuse in subsequent iterations, which efficiently mitigates errors due to imperfect photon–spin interactions. Conversely, if the photon state $|L\rangle$ does not change, it indicates a qubit-flip operation $|1\rangle \leftrightarrow |0\rangle$ in the electron-spin state of the NV$^-$–cavity system. Therefore, when the detector D$_1$ is not activated, the system becomes

$$\begin{aligned} &|L\rangle|1\rangle \to M|L\rangle|0\rangle, \quad |L\rangle|0\rangle \to M|L\rangle|1\rangle, \\ &|R\rangle|1\rangle \to M|R\rangle|1\rangle, \quad |R\rangle|0\rangle \to M|R\rangle|0\rangle. \end{aligned} \tag{6}$$

In the second step, we consider an auxiliary photon initially in the left-polarized state $|L\rangle_0$ that enters the EPPDD. The photon passes through a variable beam splitter (VBS), which acts as a non-equilibrium optical element with a transmission coefficient of $(1+M^6)^{-1/2}$ and a reflection coefficient of $M/[(1+M^6)^{1/2}]$. Subsequently, the photon in path 1 passes through the time-delay device, meanwhile the photon in path 2 progresses through a series of operations: H$_3$ $\to$ NV$^-$–cavity system $\to$ H$_4$. The system states are evolved into

$$\begin{aligned} |L\rangle_0^1 \otimes M|L\rangle|0\rangle &\to \frac{M^2}{\sqrt{1+M^6}}|L\rangle_0^1|L\rangle|0\rangle, \\ |L\rangle_0^1 \otimes M|L\rangle|1\rangle &\to \frac{M^2}{\sqrt{1+M^6}}|L\rangle_0^1|L\rangle|1\rangle, \\ |L\rangle_0^1 \otimes M|R\rangle|1\rangle &\to \frac{M^2}{\sqrt{1+M^6}}|L\rangle_0^1|R\rangle|1\rangle, \\ |L\rangle_0^1 \otimes M|R\rangle|0\rangle &\to \frac{M^2}{\sqrt{1+M^6}}|L\rangle_0^1|R\rangle|0\rangle, \end{aligned}$$

$$
\begin{aligned}
|L\rangle_0^2\otimes M|L\rangle|0\rangle \;\rightarrow\; & -\frac{M^2}{\sqrt{1+M^6}}|R\rangle_0^2|L\rangle|0\rangle \\
& +\frac{MN}{\sqrt{1+M^6}}|L\rangle_0^2|L\rangle|0\rangle, \\
|L\rangle_0^2\otimes M|L\rangle|1\rangle \;\rightarrow\; & \frac{M^2}{\sqrt{1+M^6}}|R\rangle_0^2|L\rangle|1\rangle \\
& +\frac{MN}{\sqrt{1+M^6}}|L\rangle_0^2|L\rangle|1\rangle, \\
|L\rangle_0^2\otimes M|R\rangle|1\rangle \;\rightarrow\; & \frac{M^2}{\sqrt{1+M^6}}|R\rangle_0^2|R\rangle|1\rangle \\
& +\frac{MN}{\sqrt{1+M^6}}|L\rangle_0^2|R\rangle|1\rangle, \\
|L\rangle_0^2\otimes M|R\rangle|0\rangle \;\rightarrow\; & -\frac{M^2}{\sqrt{1+M^6}}|R\rangle_0^2|R\rangle|0\rangle \\
& +\frac{MN}{\sqrt{1+M^6}}|L\rangle_0^2|R\rangle|0\rangle, \qquad (7)
\end{aligned}
$$

where the superscripts 1 and 2 denote the reflection and transmission paths, respectively. Like the first step, the photon state $|L\rangle_0^2$ consistently displays two different output modes. The left-polarized state $|L\rangle_0^2$ reflected by the $CPBS_3$ is detected by the detector D_2, which indicates the occurrence of an error. In such cases, the polarization states of the photon and the electron spin remain unchanged. Conversely, if the detector D_2 does not respond, it suggests that the photon successfully passes through the $CPBS_3$. This observation can be utilized to predict potential error occurrences. Ultimately, the auxiliary photon in state $|R\rangle_0^2$ passes through the half-wave plate X, which executes bit-flip operation on the photon, $|R\rangle \leftrightarrow |L\rangle$. After all operations, when the detector D_2 remains inactive, the entangled state of the photon in the transmission path evolves into

$$
\begin{aligned}
|L\rangle_0^2\otimes M|L\rangle|0\rangle &\rightarrow -\frac{M^2}{\sqrt{1+M^6}}|L\rangle_0^2|L\rangle|0\rangle, \\
|L\rangle_0^2\otimes M|L\rangle|1\rangle &\rightarrow \frac{M^2}{\sqrt{1+M^6}}|L\rangle_0^2|L\rangle|1\rangle, \\
|L\rangle_0^2\otimes M|R\rangle|1\rangle &\rightarrow \frac{M^2}{\sqrt{1+M^6}}|L\rangle_0^2|R\rangle|1\rangle, \\
|L\rangle_0^2\otimes M|R\rangle|0\rangle &\rightarrow -\frac{M^2}{\sqrt{1+M^6}}|L\rangle_0^2|R\rangle|0\rangle. \qquad (8)
\end{aligned}
$$

Next the two components $|L\rangle_0^1$ and $|L\rangle_0^2$ converge at the beam splitter (BS). The BS executes specific operations

$$
|L\rangle_0^1 \rightarrow (|L\rangle_0^1+|L\rangle_0^2)/\sqrt{2}, \quad |L\rangle_0^2 \rightarrow (|L\rangle_0^1-|L\rangle_0^2)/\sqrt{2}. \qquad (9)
$$

After completing the two aforementioned steps, the overall system is evolved into

$$
\begin{aligned}
|L\rangle_0|L\rangle|1\rangle &\rightarrow \frac{\sqrt{2}M^2}{\sqrt{1+M^6}}|L\rangle_0^2|L\rangle|0\rangle, \\
|L\rangle_0|L\rangle|0\rangle &\rightarrow \frac{\sqrt{2}M^2}{\sqrt{1+M^6}}|L\rangle_0^1|L\rangle|1\rangle, \\
|L\rangle_0|R\rangle|1\rangle &\rightarrow \frac{\sqrt{2}M^2}{\sqrt{1+M^6}}|L\rangle_0^1|R\rangle|1\rangle, \\
|L\rangle_0|R\rangle|0\rangle &\rightarrow \frac{\sqrt{2}M^2}{\sqrt{1+M^6}}|L\rangle_0^2|R\rangle|0\rangle. \qquad (10)
\end{aligned}
$$

In the third step, the output photon from the first step reenters the "In" path and repeats the operation of the first step, the system transforms into

$$
\begin{aligned}
|L\rangle_0|L\rangle|1\rangle &\rightarrow \frac{\sqrt{2}M^3}{\sqrt{1+M^6}}|L\rangle_0^2|L\rangle|1\rangle, \\
|L\rangle_0|L\rangle|0\rangle &\rightarrow \frac{\sqrt{2}M^3}{\sqrt{1+M^6}}|L\rangle_0^1|L\rangle|0\rangle, \\
|L\rangle_0|R\rangle|1\rangle &\rightarrow \frac{\sqrt{2}M^3}{\sqrt{1+M^6}}|L\rangle_0^1|R\rangle|1\rangle, \\
|L\rangle_0|R\rangle|0\rangle &\rightarrow \frac{\sqrt{2}M^3}{\sqrt{1+M^6}}|L\rangle_0^2|R\rangle|0\rangle. \qquad (11)
\end{aligned}
$$

Finally, the auxiliary photon in state $|L\rangle_0^1$ ($|L\rangle_0^2$) is detected by the detector $D_{1'}$ ($D_{2'}$).

We have now presented all the operational steps necessary for executing the EPPDD. The four hybrid Bell states, formed by one input photon and one electron spin, can be depicted as follows:

$$
\begin{aligned}
|\phi^{\pm}\rangle &= \frac{1}{\sqrt{2}}(|R1\rangle \pm |L0\rangle), \\
|\psi^{\pm}\rangle &= \frac{1}{\sqrt{2}}(|R0\rangle \pm |L1\rangle). \qquad (12)
\end{aligned}
$$

After completing the EPPDD operation, the entire system, with the auxiliary photon initially in the left-polarized state $|L\rangle_0$ and the input photon and electron spins initially in the hybrid Bell state, undergoes the following transformation:

$$
\begin{aligned}
|L\rangle_0|\phi^{\pm}\rangle &\xrightarrow{\text{EPPDD}} \mu|L\rangle_0^1|\phi^{\pm}\rangle, \\
|L\rangle_0|\psi^{\pm}\rangle &\xrightarrow{\text{EPPDD}} \mu|L\rangle_0^2|\psi^{\pm}\rangle, \qquad (13)
\end{aligned}
$$

where $\mu = [(2M^6/(1+M^6)]^{1/2}$. If $D_{1'}$ ($D_{2'}$) responds, the hybrid states are even (odd) parity.

4. The conversion from two-qubit KLM state to Bell states

To start with, we examine the transformation of two-qubit hybrid KLM state into Bell states. The conversion process enables us to comprehensively understand the relationship between the two types of entangled states. The hybrid KLM state, involving an input photon and an electron spin of the NV^-–cavity system, can be articulated as follows:

$$
|\Psi_0\rangle = \frac{1}{\sqrt{3}}(|R1\rangle + |L0\rangle + |R0\rangle). \qquad (14)
$$

Initially, the input photon and the auxiliary photon $|L\rangle_1$ undergo interaction with the EPPDD, as depicted in Fig. 2.

If neither detector D_1 nor D_2 triggers, the system transitions from $|\Psi_0\rangle \otimes |L\rangle_1$ into

$$|\Psi_1\rangle = \frac{\mu}{\sqrt{3}}[(|R1\rangle + |L0\rangle)|L\rangle_1^1 + |R0\rangle|L\rangle_1^2]. \quad (15)$$

When detector $D_{1'}$ responds, the Bell state $|\phi^+\rangle$ can be obtained with the probability of $2\mu^2/3$. Correspondingly, when detector $D_{2'}$ responds, the state $\frac{\mu}{\sqrt{3}}|R0\rangle$ is generated with the probability of $\mu^2/3$. Converting the entangled state $\frac{\mu}{\sqrt{3}}|R0\rangle$ into Bell states is our next goal, which can significantly enhance the utilization of hybrid qubits.

Furthermore, before proceeding with the subsequent state conversion operations, Hadamard operation H^p is performed on the input photon and Hadamard operation H^e is applied to the NV^-–cavity system using a $\pi/2$ microwave pulse, resulting in the desired transformation

$$\frac{\mu}{\sqrt{3}}|R0\rangle \xrightarrow{H^p \text{ and } H^e} \frac{\mu}{2\sqrt{3}}[(|R1\rangle - |L0\rangle) - (|R0\rangle - |L1\rangle)]. \quad (16)$$

After two Hadamard operations, the entangled state enters the EPPDD with the assistance of $|L\rangle_2$. If neither detector D_1 nor D_2 responds, the system subsequently evolves as follows:

$$|\Psi_2\rangle = \frac{\mu^2}{2\sqrt{3}}[(|R1\rangle - |L0\rangle)|L\rangle_2^1 - (|R0\rangle - |L1\rangle)|L\rangle_2^2]. \quad (17)$$

Through the analysis of Eq. (17), we can determine that when $D_{1'}$ is triggered, the Bell state $|\phi^-\rangle$ is obtained with the probability of $\mu^4/6$. Conversely, when $D_{2'}$ is triggered, the Bell state $|\psi^-\rangle$ is produced with the probability of $\mu^4/6$. The protocol efficiently converts the two-qubit hybrid KLM state into Bell states $|\phi^+\rangle$, $|\phi^-\rangle$ and $|\psi^-\rangle$ with the probabilities of $2\mu^2/3$, $\mu^4/6$ and $\mu^4/6$ using two auxiliary photons and EPPDD, achieving our anticipated goal.

5. The conversion from three-qubit KLM state to GHZ states

In addition, we will investigate the conversion of the three-qubit hybrid KLM state into GHZ states. The hybrid GHZ state is established by encoding photon A as the first qubit, photon B as the second qubit, and the electron spin as the third qubit. Eight distinct GHZ states are described as follows:

$$\begin{aligned}
|\phi^\pm\rangle_{000} &= \frac{1}{\sqrt{2}}(|RR1\rangle \pm |LL0\rangle), \\
|\phi^\pm\rangle_{001} &= \frac{1}{\sqrt{2}}(|RR0\rangle \pm |LL1\rangle), \\
|\phi^\pm\rangle_{010} &= \frac{1}{\sqrt{2}}(|RL1\rangle \pm |LR0\rangle), \\
|\phi^\pm\rangle_{100} &= \frac{1}{\sqrt{2}}(|LR1\rangle \pm |RL0\rangle).
\end{aligned} \quad (18)$$

The three-qubit hybrid KLM state is defined as follows:

$$|\Phi_0\rangle = \frac{1}{2}(|RR1\rangle + |RR0\rangle + |RL0\rangle + |LL0\rangle). \quad (19)$$

During the conversion process, we assume that D_1 and D_2 do not respond. Initially, the input photon A and the auxiliary photon $|L\rangle_1$ interact with the EPPDD, resulting in the entangled state becoming

$$\begin{aligned}
|\Phi_1\rangle = \frac{\mu}{2}&[(|RR1\rangle + |LL0\rangle)|L\rangle_1^1 \\
&+ (|RR0\rangle + |RL0\rangle)|L\rangle_1^2].
\end{aligned} \quad (20)$$

When detector $D_{1'}$ is triggered, the GHZ state $|\phi^+\rangle_{000}$ is produced with the probability of $\mu^2/2$. Similarly, when detector $D_{2'}$ activates, the entangled state $\frac{\mu}{2}(|RR0\rangle + |RL0\rangle)$ is generated with the probability of $\mu^2/2$. To convert the KLM state completely into the GHZ state, it is imperative to convert the remaining states $\frac{\mu}{2}(|RR0\rangle + |RL0\rangle)$ into the GHZ states. The Hadamard operation H^p is performed on the input photon A, and Hadamard operation H^e is applied to the NV^-–cavity system via a $\pi/2$ microwave pulse. The entangled state $\frac{\mu}{2}(|RR0\rangle + |RL0\rangle)$ undergoes the following transformation:

$$\begin{aligned}
&\frac{\mu}{2}(|RR0\rangle + |RL0\rangle) \\
\xrightarrow{H^p \text{ and } H^e}\ &\frac{\mu}{4}[(|RR1\rangle - |LL0\rangle) - (|RR0\rangle - |LL1\rangle) \\
&+ (|RL1\rangle - |LR0\rangle) + (|LR1\rangle - |RL0\rangle)].
\end{aligned} \quad (21)$$

Afterwards, the input photon B and auxiliary photon $|L\rangle_2$ interact with the EPPPD, causing the system to evolve into

$$\begin{aligned}
|\Phi_2\rangle = \frac{\mu^2}{4}&[(|RR1\rangle - |LL0\rangle + |LR1\rangle - |RL0\rangle)|L\rangle_2^1 \\
&+ (|RL1\rangle - |LR0\rangle - |RR0\rangle + |LL1\rangle)|L\rangle_2^2].
\end{aligned} \quad (22)$$

From Eq. (22), we can deduce that if detector $D_{1'}$ is triggered, the state $\frac{\mu^2}{4}(|RR1\rangle - |LL0\rangle + |LR1\rangle - |RL0\rangle)$ is obtained. Alternatively, if detector $D_{2'}$ activates, the state $\frac{\mu^2}{4}(|RL1\rangle - |LR0\rangle - |RR0\rangle + |LL1\rangle)$ is acquired.

Then the input photon B and auxiliary photon $|L\rangle_3$ ($|L\rangle_4$) interact with the EPPDD, during which the equation evolves into $|\Phi_3\rangle(|\Phi_4\rangle)$ as follows:

$$\begin{aligned}
|\Phi_3\rangle &= \frac{\mu^3}{4}[(|RR1\rangle - |LL0\rangle)|L\rangle_3^1 + (|LR1\rangle - |RL0\rangle|L\rangle_3^2], \\
|\Phi_4\rangle &= \frac{\mu^3}{6}[(|RL1\rangle - |LR0\rangle)|L\rangle_4^1 - (|RR1\rangle - |LL0\rangle)|L\rangle_4^2].
\end{aligned} \quad (23)$$

After analyzing Eq. (23), it can be determined that if detector $D_{1'}$ is triggered, the GHZ state $|\phi^-\rangle_{000}$ ($|\phi^-\rangle_{010}$) is obtained with the probability of $\mu^6/8$, alternatively, if detector $D_{2'}$ activates, the GHZ state $|\phi^-\rangle_{100}$ ($|\phi^-\rangle_{001}$) is acquired with the probability of $\mu^6/8$. Up to this point, the hybrid KLM state is fully converted to GHZ states $|\phi^+\rangle_{000}$, $|\phi^-\rangle_{000}$, $|\phi^-\rangle_{001}$, $|\phi^-\rangle_{010}$ and $|\phi^-\rangle_{100}$ with the probabilities of $\mu^2/2$, $\mu^6/8$, $\mu^6/8$, $\mu^6/8$ and $\mu^6/8$ using four auxiliary photons and EPPDDs.

6. Discussion

Within the framework of photons described as $|R\rangle$ or $|L\rangle$ at frequencies close to resonance, where $\omega \approx \omega_c$ (hence $\Delta_c \approx 0$ indicating trivial detuning), the expression for the reflection coefficient $r_s(\omega)$ simplifies to $r_s = (C - i\Delta_s - 1)/(C + i\Delta_s + 1)$. When C is significantly greater than $\max(\Delta_s, 1)$, $r_0(\omega)$ approximates to 1, and $r_1(\omega)$ reaches -1 under scenarios where $\Delta_s \gg \max(C, 1)$ or when C nears zero. In a system combining NV^- and a cavity, an R-polarized photon incident at a frequency nearly resonance with $\omega_0 \approx \omega_c$ shows notable scattering to the output. Particularly when the NV^- center is in state $|0\rangle$ or $|1\rangle$, leading to phase shifts of 0 and π, respectively, the reflection coefficients can be approximated as $r_0(\omega) \approx 1$ and $r_1(\omega) \approx -1$. These coefficients are influenced by the spin state of the NV^- center. However, factors like the coupling strength g/κ and various detunings can alter the ideal single-photon scattering scenario, influencing the accuracy of the protocols. Fortunately, problems such as photon loss through dissipation and frequency detuning can be indicated as heralded failure events by detectors, thus the fidelity of converting KLM state into Bell states and GHZ state with EPPDDs can be close to unity.

If we employ superconducting nanowire single-photon detectors (SNSPDs) with approximately 95% efficiency for D_1' and D_2', the overall efficiency of the conversion protocol would decrease to 95% of the ideal efficiency after each detection event by D_1' and D_2'. Nevertheless, the fidelity remains unchanged, as in our scheme, a non-responsive detector signifies photon loss, necessitating the reintroduction of an auxiliary photon. After accounting for the 95% efficiency of detectors D_1' and D_2', the efficiencies for converting KLM states into Bell states and GHZ states are detailed as follows: η_1 represents the efficiency of the first step for converting both two-qubit and three-qubit KLM states into Bell states and GHZ states, respectively, and is given by $\eta_1 = 95\%\mu^2$. η_2, representing the efficiency for the second conversion step for both two-qubit and three-qubit KLM states into Bell states and GHZ states respectively, is given by $\eta_2 = 95\%^2\mu^4$. The efficiency η_3, applicable only to the third step of converting a three-qubit KLM state into GHZ states, is $\eta_3 = 95\%^3\mu^6$. The overall efficiencies η_B and η_G for converting two-qubit KLM states into two-qubit Bell states and three-qubit KLM states into three-qubit GHZ states are expressed as $\eta_B = (2\eta_1 + \eta_2)/3$ and $\eta_G = (\eta_1 + \eta_3)/2$, respectively. These efficiencies are dependent on parameters g/κ, with the conditions $\gamma = 0.01\kappa$ and $\Delta_c = \Delta_s = 0$, as shown in Figs. 3. The analysis of Figs. 3 reveals that the efficiencies η_1, η_2, η_3, η_B, and η_G are significantly affected by the increase in g/κ. For example, increasing g/κ from 0.61 to 1.10 leads to efficiency increasing from 93.07%, 80.61%, 94.02%, 90.92%, and 86.84% to 94.40%, 89.12%, 84.13%, 92.64%, and 89.27%, respectively. The coupling strength must not be too large, otherwise the rotating wave approximation may not hold true.

In Ref. [90], the dead time of the SNSPD (the time interval following photon absorption during which the detector cannot reliably register a second photon) is around 10 ns. Additionally, the timing jitter of the SNSPD, which refers to the variation in the time interval between photon absorption and the generation of an output electrical pulse, is exceptionally low at 65 ps. Therefore, the time required for the detector to complete a single measurement is approximately 10 ns. Our protocol requires a maximum of three single-photon measurements. Given the long coherence time of electron spin in NV center, the entanglement should remain robust and persist for a considerable duration (approximately 1 μs). Consequently, the total measurement time is significantly shorter than the electron spin's coherence time, ensuring the successful implementation of the state conversion protocol. In a practical setting, our scheme can achieve more robust operation by detecting output pulses with single-photon detectors. In this way, all sources of photon loss, including spontaneous emission, cavity mirror absorption and scattering, imperfections in the photon source, and insufficient photon collection and detection efficiency, will be flagged by the absence of photon counts. As a result, photon loss errors in the actual system will not affect the fidelities of the conversion schemes, but the efficiencies of the conversion will be impacted.

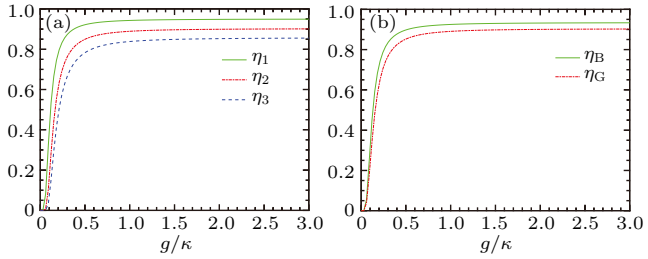


Fig. 3. (a) The efficiency η_1 (η_2 and η_3) of the first (second and third) step of the conversion from KLM to Bell states and GHZ states. (b) The total efficiency η_B (η_G) of converting KLM state into Bell states (GHZ states) vs. the coupling strength g/κ with $\gamma = 0.01\kappa$ and $\Delta_c = \Delta_s = 0$.

7. Conclusion

In conclusion, we introduce two methods for converting hybrid KLM states to Bell and GHZ states with the aid of photons. Our approaches utilize quantum circuits implemented by EPPDD across different conversion stages, ensuring reliability through the interaction of the NV^-–cavity system with a single photon. The actual scattering of photons, marked by potential mismatches in the coupling between the NV^-–cavity system and the cavity mode, is identified by single detector activations. Our analysis indicates that enhancements in coupling strength lead to greater efficiencies in these conversion processes.

Acknowledgements

This work was supported by the National Key R&D Program of China (Grant No. 2022YFB3203400), the National Natural Science Foundation of China (Grant No. 61901420), and Fundamental Research Program of Shanxi Province (Grant No. 20230302121116).

References

[1] Wehner S, Elkouss D and Hanson R 2018 *Science* **362** eaam9288
[2] Georgescu I M, Ashhab S and Nori F 2014 *Rev. Mod. Phys.* **86** 153
[3] Xu L, Wang L X, Chen G J, Chen L, Yang Y H, Xu X B, Liu A P, Li C F, Guo G C and Zou C L 2023 *Chin. Phys. Lett.* **40** 9
[4] Li T, Gao Z K and Li Z H 2020 *Europhys. Lett.* **131** 60001
[5] Li T and Long G L 2020 *New J. Phys.* **22** 063017
[6] Deng F G, Long G L and Liu X S 2003 *Phys. Rev. A* **68** 042317
[7] Su S L, Wang C, Song P Y and Chen G 2024 *Chin. Phys. Lett.* **41** 4
[8] Cirac J I, Ekert A K , Huelga S F and Macchiavello C 1999 *Phys. Rev. A* **59** 4249
[9] Lim Y L, Beige A and Kwek L C 2005 *Phys. Rev. Lett.* **95** 030505
[10] Qin W, Wang X, Miranowicz A, Zhong Z and Nori F 2017 *Phys. Rev. A* **96** 012315
[11] Cohen I and Mølmer K 2018 *Phys. Rev. A* **98** 030302
[12] Luo G F, Zhou R G and Hu W W 2019 *Chin. Phys. B* **28** 040302
[13] Yang L, Liu Y C and Li Y S 2020 *Chin. Phys. B* **29** 060301
[14] Ekert A K 1991 *Phys. Rev. Lett.* **67** 661
[15] Bennett C H and Brassard G 2014 *Theor. Comput. Sci.* **560** 7
[16] Li J J, Wang Y, Li H W and Bao W S 2020 *Chin. Phys. B* **29** 030303
[17] Zhao Y B, Zhang W L, Wang D, Song X T, Zhou L J and Ding C B 2019 *Chin. Phys. B* **28** 104203
[18] Wang Z Q and Wang T J 2023 *Phys. Rev. A* **108** 012434
[19] Gangopadhyay S, Wang T, Mashatan A and Ghose S 2022 *Phys. Rev. A* **106** 052433
[20] Wang T J, Yang G Q and Wang C 2020 *Phys. Rev. A* **101** 012323
[21] Hong Y P, Zhou L, Zhong W and Sheng Y B 2023 *Quantum Inf. Process.* **22** 111
[22] Zhang W, Ding D S, Sheng Y B, Zhou L, Shi B S and Guo G C 2017 *Phys. Rev. Lett.* **118** 220501
[23] Zhu F, Zhang W, Sheng Y B and Huang Y D 2017 *Sci. Bull.* **62** 1519
[24] Zhao P, Zhong W, Du M M, Li X Y, Zhou L and Sheng Y B 2024 *Front. Phys.* **19** 51201
[25] Sun Z Z, Pan D, Ruan D and Long G L 2023 *J. Lightwave Technol.* **41** 4680
[26] Li X J, Pan D, Long G L and Hanzo L 2023 *IEEE Commun. Lett.* **27** 1060
[27] Long G L and Liu X S 2002 *Phys. Rev. A* **65** 032302
[28] Zhou L, Xu B W, Zhong W and Sheng Y B 2023 *Phys. Rev. Appl.* **19** 014036
[29] Qian P and Liu D 2023 *Chin. Phys. Lett.* **40** 10
[30] Li C, Zhou L, Zhong W and Sheng Y B 2022 *Quantum Inf. Process.* **21** 178
[31] Qi Z T, Li Y H, Huang Y W, Feng J, Zheng Y L and Chen X F 2021 *Light Sci. Appl.* **10** 183
[32] Long G L and Zhang H R 2021 *Sci. Bull.* **66** 1267
[33] Pan D, Song X T and Long G L 2023 *Adv. Devices Instrum.* **4** 0004
[34] Zheng S B 2001 *Phys. Rev. Lett.* **87** 230404
[35] Walther P, Resch K J and Zeilinger A 2005 *Phys. Rev. Lett.* **94** 240501
[36] Knill E, Laflamme R and Milburn G J 2001 *Nature* **409** 46
[37] Agrawal P and Pati A 2006 *Phys. Rev. A* **74** 062320
[38] Shen C P, Gu X F, Guo Q, Zhu X Y, Su S L and Liang E 2018 *J. Opt. Soc. Am. B* **35** 694
[39] Du F F and Shi Z R 2019 *Opt. Express* **27** 17493
[40] Ou Z Y and Mandel L 1988 *Phys. Rev. Lett.* **61** 50
[41] Pan J W, Daniell M, Gasparoni S, Weihs G and Zeilinger A 2001 *Phys. Rev. Lett.* **86** 4435
[42] Zheng R H, Kang Y H, Shi Z C and Xia Y 2019 *Ann. Phys.* **531** 1800447
[43] Dur W, Vidal G and Cirac J I 2000 *Phys. Rev. A* **62** 062314
[44] Bugu S, Yesilyurt C and Ozaydin F 2013 *Phys. Rev. A* **87** 032331
[45] Du F F, Fan G, Ren X M and Ma M 2023 *Adv. Quantum Technol.* **6** 2300201
[46] Du F F, Ren X M, Fan Z G, Li L H, Du X S, Ma M, Fan G and Guo J 2024 *Opt. Express* **32** 1686
[47] Acín A, Bruß D, Lewenstein M and Sanpera A 2001 *Phys. Rev. Lett.* **87** 040401
[48] Du F F, Ma M and Tan Q L 2024 *Adv. Quantum Technol.* 2400322
[49] Shen C P, Gao Y, Su S L, Mao Y, Liang E and Chen S 2018 *Ann. Phys.* **530** 1800114
[50] Song J, Sun X D, Mu Q X, Zhang L L, Xia Y and Song H S 2013 *Phys. Rev. A* **88** 024305
[51] Tashima T, Wakatsuki T, Özdemir Ş K, Yamamoto T, Koashi M and Imoto N 2009 *Phys. Rev. Lett.* **102** 130502
[52] Shen C P, Xiu X M, Dong L, Zhu X Y, Chen L, Liang E, Yan L L and Su S L 2019 *Ann. Phys.* **531** 1900160
[53] Chen L, Xiu X M, Dong L, Zhang S, Su S L, Chen S and Liang E J 2021 *Ann. Phys.* **534** 2100365
[54] Du F F, Ren X M, Ma M and Fan G 2023 *Appl. Phys. Express* **16** 102006
[55] Gaebel T, Domhan M, Popa I, *et al.* 2006 *Nat. Phys.* **2** 408
[56] Fuchs G D, Dobrovitski V V, Toyli D M, Heremans F J and Awschalom D D 2009 *Science* **326** 1520
[57] Englund D, Shields B, Rivoire K, Hatami F, Vuckovic J, Park H and Lukin M D 2010 *Nano Lett.* **10** 3922
[58] Zhang J F and Suter D 2015 *Phys. Rev. Lett.* **115** 110502
[59] Robledo L, Childress L, Bernien H, Hensen B, Alkemade P F A and Hanson R 2011 *Nature* **477** 574
[60] Dutt M V G, Childress L, Jiang L, Togan E, Maze J, Jelezko F, Zibrov A S, Hemmer P R and Lukin M D 2007 *Science* **316** 1312
[61] Shi F Z, Rong X, Xu N Y, *et al.* 2010 *Phys. Rev. Lett.* **105** 040504
[62] Du F F, Liu Y T, Shi Z R, Liang Y X, Tang J and Liu J 2019 *Opt. Express* **27** 27046
[63] Sar T, Wang Z H, Blok M S, *et al.* 2012 *Nature* **484** 82
[64] Arroyo-Camejo S, Lazariev A, Hell S W and Balasubramanian G 2014 *Nat. Commun.* **5** 4870
[65] Zu C, Wang W B, He L, Zhang W G, Dai C Y, Wang F and Duan L M 2014 *Nature* **514** 72
[66] Togan E, Chu Y, Trifonov A S, *et al.* 2010 *Nature* **466** 730
[67] Du F F and Ren X M 2025 *Opt. Laser Technol.* **114** 053603
[68] Kosaka H and Niikura N 2015 *Phys. Rev. Lett.* **180** 111440
[69] Ren X M and Du F F 2024 *Adv. Quantum Technol.* 2400208
[70] Du F F, Fan G and Ren X M 2024 *Quantum* **8** 1342
[71] Bernien H, Hensen B, Pfaff W, Koolstra G, Blok M S, Robledo L, Taminiau T H, Markham M, Twitchen D J, Childress L and Hanson R 2013 *Nature* **497** 86
[72] Wu Y M, Fan G and Du F F 2022 *Front. Phys.* **17** 51502
[73] Du F F, Ren X M and Guo J 2024 *Opt. Express* **32** 31633
[74] Wei H R and Long G L 2015 *Phys. Rev. A* **91** 032324
[75] Ren B C and Deng F G 2013 *Laser Phys. Lett.* **10** 115201
[76] Du F F, Wu Y M and Fan G 2023 *Adv. Quantum Technol.* **6** 2300090
[77] Wang T J and Wang C 2014 *Phys. Rev. A* **90** 052310
[78] Du F F, Ren X M, Ma M and Fan G 2024 *Opt. Lett.* **49** 1229
[79] Wang C, Zhang Y, Jiao R Z and Jin G S 2013 *Opt. Express* **21** 19252
[80] Jiang L, Taylor J M, Sørensen A S and Lukin M D 2007 *Phys. Rev. A* **76** 062323
[81] Reiserer A and Rempe G 2015 *Rev. Mod. Phys.* **87** 1379
[82] Nemoto K, Trupke M, Devitt S J, Stephens A M, Scharfenberger B, Buczak K, Nöbauer T, Everitt M S, Schmiedmayer J and Munro W J 2014 *Phys. Rev. X* **4** 031022
[83] Doherty M W, Dolde F, Fedder H, Jelezko F, Wrachtrup J, Manson N B and Hollenberg L C L 2012 *Phys. Rev. B* **85** 205203
[84] Du F F, Ren X M and Tan Q L 2024 *Adv. Quantum Technol.* 2400313
[85] Astner T, Nevlacsil S, Peterschofsky N, Angerer A, Rotter S, Putz S, Schmiedmayer J and Majer J 2017 *Phys. Rev. Lett.* **118** 140502
[86] Kalhor F, Yang L P, Bauer L and Jacob Z 2021 *Phys. Rev. Res.* **3** 043007
[87] Hu C Y, Young A, O'Brien J L, Munro W J and Rarity J G 2008 *Phys. Rev. B* **78** 085307
[88] An J H, Feng M and Oh C H 2009 *Phys. Rev. A* **79** 032303
[89] Lodahl P, Mahmoodian S and Stobbe S 2015 *Rev. Mod. Phys.* **87** 347
[90] Hadfield R 2009 *Nat. Photonics* **3** 696